


 CrossMark  
click for updates

 Cite this: *CrystEngComm*, 2015, 17, 8500

## *In situ* X-ray diffraction study on the formation of $\alpha$ -Sn in nanocrystalline Sn-based electrodes for lithium-ion batteries†

 Nikolas Oehl,<sup>\*a</sup> Guido Schmuelling,<sup>\*b</sup> Martin Knipper,<sup>a</sup> Richard Kloepsch,<sup>b</sup> Tobias Placke,<sup>b</sup> Joanna Kolny-Olesiak,<sup>a</sup> Thorsten Plaggenborg,<sup>a</sup> Martin Winter<sup>b</sup> and Juergen Parisi<sup>a</sup>

*In situ* X-ray diffraction (XRD) was performed to study the formation of the  $\alpha$ -Sn structure in nanocrystalline Sn-based electrodes during electrochemical lithium insertion and extraction at room temperature. Therefore, pure  $\beta$ -Sn nanoparticles were synthesised and further processed into electrodes. The lithiation and de-lithiation process of the  $\beta$ -Sn nanoparticles follows the formation of discrete lithium-tin phases which perfectly fits the voltage plateaus in the charge/discharge diagram. However, unlike bulk electrodes, where no  $\alpha$ -Sn is formed, we observed the formation of the semiconducting  $\alpha$ -modification at 870 mV vs. Li within the first de-lithiation process. This observation explains earlier reports of an increasing internal resistance of such an electrode. Additionally, our study supports earlier suggestions that predominantly small tin crystallites are transformed from the  $\beta$ -Sn phase into the  $\alpha$ -Sn phase, while larger crystallites retain their metallic  $\beta$ -Sn structure.

 Received 16th September 2015,  
Accepted 5th October 2015

DOI: 10.1039/c5ce01841b

[www.rsc.org/crystengcomm](http://www.rsc.org/crystengcomm)

### Introduction

In order to increase the specific energy (Wh kg<sup>-1</sup>) and energy density (Wh L<sup>-1</sup>) of lithium-ion batteries, there is a need for high-capacity anode materials to replace graphitic carbons as state-of-the-art negative electrode materials. Apart from silicon,<sup>1</sup> tin is a promising anode material due to its high gravimetric (959 mAh g<sup>-1</sup>) and volumetric (2000 mAh cm<sup>-3</sup>) capacities.<sup>2</sup> Tin nanoparticles can be transformed from the metallic  $\beta$ -Sn into the semiconducting  $\alpha$ -Sn structure at room temperature when cycled in a lithium-ion battery.<sup>3–7</sup> Kim *et al.*<sup>3</sup> reported the existence of cubic Sn ( $\alpha$ -Sn) in small (3–8 nm) nanoparticles after 30 cycles in a lithium-ion cell. Furthermore, Xu *et al.*<sup>4</sup> investigated the mechanical damage of 10 nm sized Sn nanocrystals during electrochemical reactions with lithium using *ex situ* high-resolution transmission electron microscopy (HR-TEM). Their findings show that the Sn nanocrystals were transformed from the tetragonal  $\beta$ -Sn phase to the cubic  $\alpha$ -Sn after lithium insertion and extraction. The authors concluded that the stability of the polymorphs  $\alpha$ -/ $\beta$ -Sn could be affected by the size of the crystallites. Such

size-dependent phase transformations are well-documented in the literature, especially for oxides like TiO<sub>2</sub> or Al<sub>2</sub>O<sub>3</sub>.<sup>8,9</sup> Im *et al.*<sup>5</sup> studied the phase evolution of Sn nanocrystals (7 nm) embedded in a carbon matrix during long-term cycling. They pointed out that the  $\alpha$ -/ $\beta$ -Sn ratio increases with respect to the cycle number. Finally, Oehl *et al.*<sup>7</sup> investigated at what crystallite size the Sn nanoparticles are transformed from the  $\beta$  structure to the  $\alpha$  structure. The critical size was determined to be 17(4) nm for  $\beta$ -Sn nanocrystals at room temperature. However, these investigations did not address the question, when does the transformation occur? Furthermore, these studies did not deal with the lithiation of the  $\alpha$ -Sn phase.

*In situ* X-ray diffraction (XRD) measurements by Rhodes *et al.*<sup>10</sup> on bulk Sn electrodes showed that the lithiation and de-lithiation process follows the formation of discrete lithium-tin phases. The presence of four phases including  $\beta$ -Sn, Li<sub>2</sub>Sn<sub>5</sub>,  $\beta$ -LiSn and Li<sub>22</sub>Sn<sub>5</sub>, which were formed during lithiation and de-lithiation, was identified and could be correlated to the voltage plateaus in the charge/discharge profile. In their work, no  $\alpha$ -Sn phase formation was observed.

In this study, we investigated the first-cycle lithiation and de-lithiation process of Sn/SnO<sub>x</sub> core/shell nanoparticles using an *in situ* XRD technique in order to get an insight into the mechanism of the  $\alpha$ -Sn formation. The *in situ* XRD measurements show that the lithiation/de-lithiation process follows the formation of lithium-tin phases similar to those in Sn bulk electrodes. However, in contrast to the bulk material, the  $\alpha$ -Sn phase is formed at the end of the first de-lithiation

<sup>a</sup> University of Oldenburg, Energy and Semiconductor Research Laboratory, Institute of Physics, Carl-von-Ossietzky-Str. 9-11, 26129 Oldenburg, Germany. E-mail: nikolas.oehl@uni-oldenburg.de

<sup>b</sup> University of Muenster, MEET Battery Research Center, Institute of Physical Chemistry, Corrensstr. 46, 48149 Muenster, Germany

† Electronic supplementary information (ESI) available: Cif data of  $\beta$ -Sn and  $\alpha$ -Sn nanoparticle crystal structures. See DOI: 10.1039/c5ce01841b



process at 870 mV vs. Li. Furthermore, the measurements show that the  $\alpha$ -Sn phase gets lithiated contemporaneous with the  $\beta$ -Sn phase, forming the same Li-Sn phases.

## Experimental methods

Sn nanoparticles with a volume-weighted mean diameter of 24 nm ( $D_{4,3} = 24$  nm) were synthesized following a method reported in one of our previous studies.<sup>11</sup> Briefly, 10 g of polyvinylpyrrolidone (PVP, M.W. 40 000 g mol<sup>-1</sup>, Alfa Aesar) and 3.5 g of SnCl<sub>2</sub> (99%, Sigma-Aldrich) were dissolved at room temperature in 900 mL of tetraethylene glycol (TEG, 99% Alfa Aesar). The stirred solution was heated up to 120 °C using the Schlenk technique under an argon atmosphere. A freshly prepared solution of 9 g of sodium borohydride (NaBH<sub>4</sub>, 99%, Acros) in 100 mL of TEG was added dropwise to the stirred SnCl<sub>2</sub> solution. The nanoparticle solution was cooled down to room temperature and diluted with acetone in order to isolate the prepared nanoparticles. The nanoparticles were dispersed and stored in ethanol.

XRD investigations were performed using a Bruker D8 Advance X-ray diffractometer (Bruker AXS GmbH) equipped with a copper target X-ray tube ( $\lambda = 1.54$  Å). *In situ* XRD analysis of the Sn active material upon galvanostatic cycling was carried out using a self-designed *in situ* cell, which has been described previously.<sup>12</sup> An electrode paste consisting of 80 wt% Sn nanoparticles, a 12 wt% conductive carbon agent Super C65 (Imerys) and 8 wt% sodium carboxymethylcellulose (Na-CMC) as a binder (Walocel CRT 2000 PPA 12, Dow Wolff Cellulosics) was applied onto a beryllium (Be) window serving as both the current collector and the X-ray transparent window. Metallic lithium foil (Rockwood Lithium) served as a counter electrode, Whatman glass fiber (grade GF/D) as a separator and 1 M LiPF<sub>6</sub> in EC/DEC 3 : 7 (by weight) with 2 wt% VC (UBE) as an electrolyte. After resting, the cell was galvanostatically cycled at a current rate of C/15 (based on the tin active weight  $m = 6.52$  mg, theoretical specific capacity = 950 mAh g<sup>-1</sup>) between 0.025 V and 1.5 V with a constant voltage step at the lower cut-off voltage ( $I \leq C/20$ ). Simultaneously, XRD measurements were performed in the  $2\theta$  angular range of 21–81° with a step size of 0.015 degrees and a step time of 0.7 s, resulting in 50 minutes per XRD scan at an accelerating voltage of 40 kV and a current of 40 mA. The Rietveld refinement of the diffraction pattern was applied with the Maud software 2.4.9 in the  $2\theta$  angular range of 21–47°. The crystal structure parameters for the  $\beta$ -Sn (03-065-7657) and the  $\alpha$ -Sn (01-087-0794) phases were taken from the ICDD database. A polynomial of the fourth degree was used to refine the background; the incident intensity factor, lattice constants and crystallite size and strain were refined in the second and third steps.

## Results and discussion

TEM and XRD measurements reveal that the as-prepared Sn nanoparticles are spherical (see Fig. 1a) and consist of a

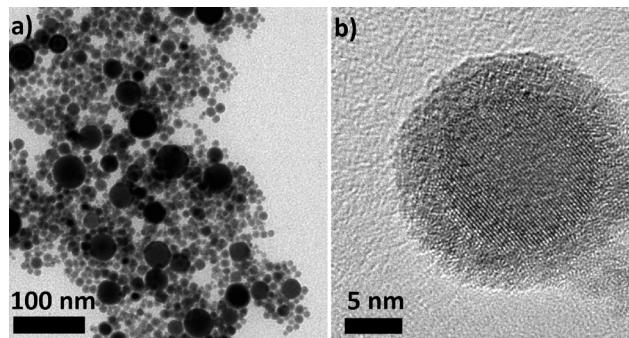


Fig. 1 a) TEM and b) HR-TEM images of the prepared Sn/SnO<sub>x</sub> core/shell nanoparticles.

crystalline  $\beta$ -Sn core and a small amorphous SnO<sub>x</sub> shell (see Fig. 1b). The nanoparticles show a broad size distribution from 5 nm to 40 nm (see Fig. 1a). This size distribution is well suited for the study of the lithiation of  $\beta$ -Sn as well as the lithiation of the  $\alpha$ -Sn phase which is already formed in the first cycle.

The size distribution was determined by TEM measurements and reveals a mean diameter of 9.8 nm and a volume-weighted mean diameter of 24 nm. The volume-weighted mean diameter was calculated according to eqn (1):

$$D_v = \frac{\sum d^4}{\sum d^3} \quad (1)$$

This size is large enough to get strong reflections for the *in situ* X-ray diffraction measurements and it is small enough to observe the desired  $\beta/\alpha$ -phase transformation.

Rietveld refinement with the Maud software version 2.3.3 was applied in order to analyse the diffraction pattern of the as-prepared nanoparticles. The crystal structures of Sn and SnO were considered to calculate the diffraction pattern. Fig. 2 shows the result of the refinement.

All strong reflections in this pattern could be assigned to the  $\beta$ -Sn phase. A broad peak at  $2\theta$  between 30° and 35° can

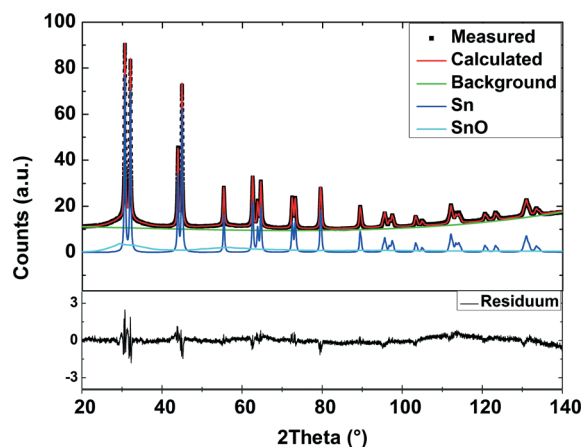


Fig. 2 XRD measurement of the prepared Sn/SnO<sub>x</sub> nanoparticles and the result of the Rietveld refinement. The weighted *R* factor is 2.1%.



be explained with the  $\text{SnO}_x$  phase. This strong broadening results from the small crystalline domains of that phase. Therefore we conclude that the nanoparticles consist of a crystalline  $\beta$ -Sn core and a  $\text{SnO}_x$  shell with only very small crystalline domains. This conclusion is supported by HR-TEM measurements (Fig. 1b) which show a highly crystalline core and an amorphous shell. The results from the refinement of the diffraction pattern of the as-prepared nanoparticles are in good agreement with the TEM measurements. Fig. 3 shows the volume-weighted size distribution of the as-prepared Sn nanoparticles. According to earlier observations, at a critical size of 17(4) nm, 33(7) wt% of the particles should be transformed into the  $\alpha$ -modification after electrochemical lithium insertion and extraction. The X-ray diffraction patterns of the *in situ* XRD measurement and the corresponding voltage profile of the first charge/discharge cycle are displayed in Fig. 4. The results show that the lithiation process follows the formation of discrete lithium-tin phases, which is perfectly correlated to the voltage plateaus from the charge/discharge profile. The lithiation process follows the formation of the same lithium-tin phases which are formed in bulk Sn-based electrodes, *i.e.*  $\text{Li}_2\text{Sn}_5$ ,  $\text{LiSn}$  and  $\text{Li}_{22}\text{Sn}_5$ .<sup>10</sup> At the beginning, the assembled *in situ* cell has an initial open circuit voltage of 2.78 V and the diffraction pattern only shows the reflections from  $\beta$ -Sn (Fig. 4a) and the (100) reflection originating from the Be window at  $2\theta = 46.1^\circ$ . The transformation of the  $\text{SnO}_x$  shell into the  $\text{Li}_2\text{O}$  phase is not observed in the X-ray diffraction measurements because of the small crystalline domain of the shell and the small scattering cross-section between X-rays and light elements. Nevertheless, a small voltage plateau at 0.9 V indicates such a transformation. When the cell voltage reaches the first plateau at 0.56 V, the reflections from the  $\beta$ -Sn phase vanish and a crystalline  $\text{Li}_2\text{Sn}_5$  (Fig. 4b) phase is formed. Shortly after the voltage falls below 0.42 V, the reflections from  $\text{Li}_2\text{Sn}_5$  disappear and the signals of the  $\text{LiSn}$  (Fig. 4c) phase appear. Once the voltage decreases below 0.31 V, the characteristic reflections<sup>13,14</sup> (a broad reflection at  $22^\circ$  and a sharp one at  $38^\circ$ ) of the highest lithiated phase  $\text{Li}_{22}\text{Sn}_5$  (Fig. 4d)

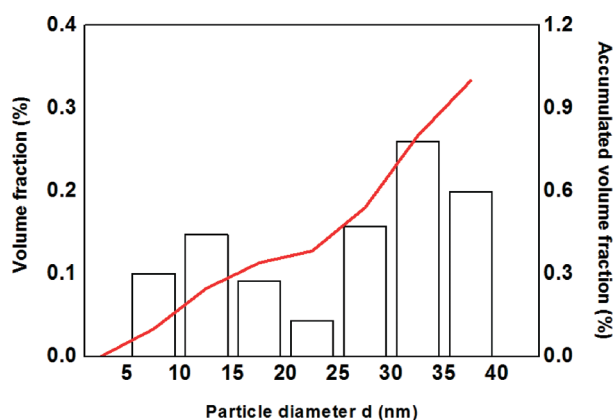


Fig. 3 Volume-weighted size histogram of the prepared tin nanoparticles determined by TEM measurements.

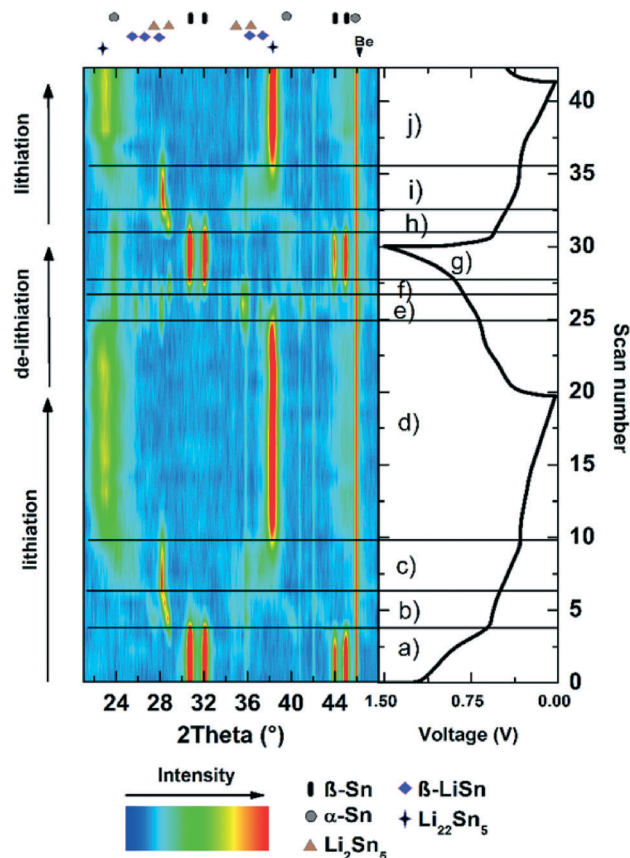


Fig. 4 Isoplot of the *in situ* XRD measurement taken during the first charge/discharge cycle of the Sn nanoparticle-based electrode. Characteristic reflections of the relevant phases are marked. The voltage profile is plotted to the right, and black lines are drawn to denote phase transformation. Phase transformations are labelled with (a) to (j) and explained in the text.

occur. In some literature reports,  $\text{Li}_{17}\text{Sn}_4$  was identified as the highest lithiated phase.<sup>15</sup> Nevertheless, the  $\text{Li}_{17}\text{Sn}_4$  crystal structure does not fit the XRD pattern from the highest electrochemically lithiated Sn phase in our experiment.

During de-lithiation (Fig. 4d–g), the same lithium-tin phases appear and vanish in reverse order and with more overlap between diffraction peaks representing the various phases. However, an uprising phase can still be correlated to a new plateau in the voltage profile. When the voltage exceeds 0.87 V, the reflections from  $\beta$ -Sn return, and additionally, the reflections from  $\alpha$ -Sn (Fig. 4g) appear as well. In the following cycles (Fig. 4h–j), the signals from the  $\alpha$ -Sn phase appear and vanish contemporaneous with the  $\beta$ -Sn phase, indicating that the  $\alpha$ -Sn phase gets lithiated and de-lithiated in a similar way as the  $\beta$ -Sn phase. Fig. 5 shows the XRD patterns and the result of the structural Rietveld refinement for the measurement before and after the first charge/discharge cycle. Fig. 5a shows the XRD pattern before the lithiation process starts. All detectable reflections can be assigned to the  $\beta$ -Sn phase and the Be window. After one complete cycle (see Fig. 5b), three additional reflections appear. These reflections can be explained by the formation



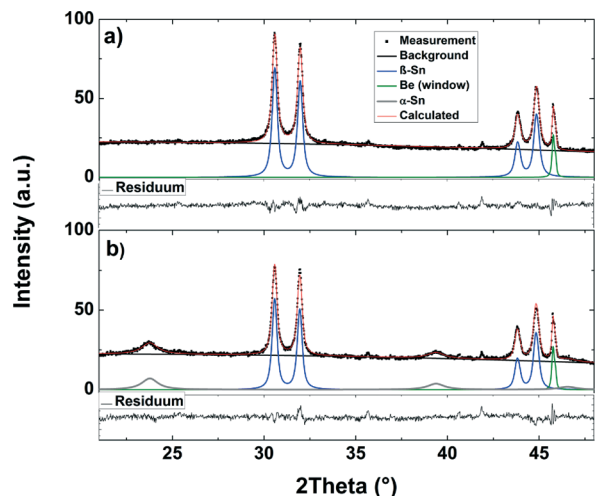


Fig. 5 XRD measurement and refinement of the nano-Sn-based electrode before (a) and after (b) the first charge/discharge cycle.

of the  $\alpha$ -Sn phase. The results of the refinement are summarized in Table 1.

The results of the refinement show that the crystallites of the  $\alpha$ -Sn phase ( $L = 7.1(4)$  nm) are significantly smaller than the crystallites of the  $\beta$ -Sn phase ( $L = 26(2)$  nm). The mean crystallite size of the  $\beta$ -Sn nanoparticles increases. Therefore we believe that the original size distribution is split into  $\alpha$ - and  $\beta$ -phase distributions. This observation is in conformity with earlier reports that the  $\beta$ -/ $\alpha$ -phase equilibrium depends on the size of the crystallites.<sup>7</sup> From the ratio of the peak intensities, we calculated the weight ratio. Therefore, after one complete cycle, the crystalline part of the Sn nanoparticles consists of 19(1) wt%  $\alpha$ -Sn and 81(1) wt%  $\beta$ -Sn. On the assumption that only the smallest particles in this distribution are transformed into the  $\alpha$ -phase, one could calculate a critical size of 11(3) nm for the transformation. Our measurements show for the first time that the  $\alpha$ -Sn phase is already formed during the first charge/discharge cycle at 870 mV and simultaneously with the  $\beta$ -phase.

Although the size-dependent phase transformation is very common for nanoparticle crystal structures, the phase transformation for Sn nanocrystals is poorly studied so far. Im *et al.*<sup>5</sup> used *ab initio* calculations to study the emergence of the  $\alpha$ -phase. They concluded that once the  $\alpha$ -phase is formed, it preserves its crystal structure, while the  $\beta$ -phase is easily transformed into an amorphous phase during lithiation. Nevertheless, the formation of the  $\alpha$ -phase is still

supposed to be a size-related effect, which is not fully understood, so far. Besides the contribution of the surface energy, the formation and the stability of  $\alpha$ -Sn depends on other factors as well. Gallerneault *et al.*<sup>16</sup> showed that small amounts (0.6 wt%) of Si can enhance the  $\alpha$ -phase stability. Furthermore, a matrix is able to stabilize the  $\alpha$ -Sn phase up to a melting point of 200 °C.<sup>17</sup> However, there are no reports about the  $\alpha$ -phase in Sn nanoparticles without the participation of lithium. Therefore, a lithium contribution to the  $\alpha$ -phase formation should be considered as well. How the size of the crystallites, the incorporation of lithium and the matrix stabilization might affect the  $\alpha$ -phase formation needs to be studied in future work.

Furthermore, the influence of the  $\alpha$ -phase on the overall electrochemical performance of Sn-based anode materials needs to be examined more carefully. For example, Im *et al.*<sup>5</sup> reported that crystalline  $\alpha$ -Sn can lead to improved rate performance. However,  $\alpha$ -Sn is a semiconductor and may lead to an increased internal resistance compared to metallic  $\beta$ -Sn. Studies by Kaghazchi<sup>18–20</sup> showed that the insertion of Li in  $\alpha$ -Sn is kinetically more favorable than that in  $\beta$ -Sn. Nevertheless, our measurements show that the  $\alpha$ -phase gets lithiated contemporaneous with the  $\beta$ -Sn phase. Therefore the kinetic influence of Li insertion into the  $\alpha$ -Sn phase seems to be negligible. Therefore, the insertion of lithium into the  $\alpha$ -Sn phase and the effect of an increased electrical resistance need to be investigated more carefully and will be the topic of our future work.

## Conclusions

In conclusion, we could show for the first time by an *in situ* X-ray diffraction study that the  $\alpha$ -Sn phase is already formed within the first cycle in a nano-particulate tin anode. The  $\alpha$ -phase is formed simultaneously with the  $\beta$ -Sn phase at a voltage of 870 mV. This  $\alpha$ -phase gets lithiated in the next cycles similar to the  $\beta$ -Sn phase. Furthermore, earlier observations about a critical size of 17(4) nm could be confirmed within the experimental error. Although it is well known that unusual phase transformations in nanoparticles are size related, one should consider that lithium insertion/extraction affects the formation and stability of the  $\alpha$ -phase. The impact of the  $\alpha$ -phase on the electrochemical performance of tin-based anodes in a lithium-ion cell should be the topic of future research to gain a deeper insight into this only little studied phase transformation.

Table 1 Summarized structural data from the Rietveld refinement in Fig. 5

	$\beta$ -Sn			$\alpha$ -Sn			$R_{wp}^b$ (%)
	$a$ (Å)	$c$ (Å)	$L$ (nm) <sup>c</sup>	$a$ (Å)	$L$ (nm)	$w_\alpha/w_\beta^a$	
As prepared	5.8388(1)	3.186(1)	24.6(9)	—	—	—	3.5
After the 1st cycle <sup>d</sup>	5.8393(1)	3.188(1)	26(2)	6.467(1)	7.1(4)	0.23	3.4

<sup>a</sup>  $w_\alpha/w_\beta$  denotes the weight ratio of the  $\alpha$ -phase/ $\beta$ -phase. <sup>b</sup>  $R_{wp}$  denotes the weighted  $R$  factor. <sup>c</sup>  $L$  denotes the crystallite size. <sup>d</sup> In the delithiated state.



## Acknowledgements

The authors gratefully acknowledge the funding of the EWE-Nachwuchsgruppe by EWE AG Oldenburg. Guido Schmuelling gratefully acknowledges the funding of the project "Pouch-Zelle" (funding code: 64.65.69-EM 1024 C) by the state NRW within the NRW Ziel 2-Programm (EFRE), Germany.

## Notes and references

- 1 W.-R. Liu, Y.-C. Yen, H.-C. Wu, M. Winter and N.-L. Wu, *J. Appl. Electrochem.*, 2009, **39**, 1643–1649.
- 2 M. Winter, J. O. Besenhard, J. H. Albering, J. Yang and M. Wachtler, *Prog. Batteries Battery Mater.*, 1998, **17**, 208–213.
- 3 C. Kim, M. Noh, M. Choi, J. Cho and B. Park, *Chem. Mater.*, 2005, **17**, 3297–3301.
- 4 L. Xu, C. Kim, A. K. Shukla, A. Dong, T. M. Mattox, D. J. Milliron and J. Cabana, *Nano Lett.*, 2013, **13**, 1800–1805.
- 5 H. S. Im, Y. J. Cho, Y. R. Lim, C. S. Jung, D. M. Jang, J. Park, F. Shojaei and H. S. Kang, *ACS Nano*, 2013, **7**, 11103–11111.
- 6 G. Schmuelling, N. Oehl, M. Knipper, J. Kolny-Olesiak, T. Plaggenborg, H.-W. Meyer, T. Placke, J. Parisi and M. Winter, *Nanotechnology*, 2014, **25**, 355401.
- 7 N. Oehl, L. Hardenberg, M. Knipper, J. Kolny-Olesiak, J. Parisi and T. Plaggenborg, *CrystEngComm*, 2015, **17**, 3695–3700.
- 8 J. M. McHale, A. Auroux, A. J. Perrotta and A. Navrotsky, *Science*, 1997, **277**, 788–791.
- 9 A. Navrotsky, *ChemPhysChem*, 2011, **12**, 2207–2215.
- 10 K. J. Rhodes, R. Meisner, M. Kirkham, N. Dudney and C. Daniel, *J. Electrochem. Soc.*, 2012, **159**, A294–A299.
- 11 N. Oehl, P. Michalowski, M. Knipper, J. Kolny-Olesiak, T. Plaggenborg and J. Parisi, *J. Phys. Chem. C*, 2014, **118**, 30238–30243.
- 12 H. Jia, C. Stock, R. Kloepsch, X. He, J. P. Badillo, O. Fromm, B. Vortmann, M. Winter and T. Placke, *ACS Appl. Mater. Interfaces*, 2015, **7**, 1508–1515.
- 13 J. R. Dahn, I. A. Courtney and O. Mao, *Solid State Ionics*, 1998, **111**, 289–294.
- 14 I. A. Courtney and J. R. Dahn, *J. Electrochem. Soc.*, 1997, **144**, 2045–2052.
- 15 C. Lupu, J.-G. Mao, J. W. Rabalais, A. M. Guloy and J. W. Richardson, *Inorg. Chem.*, 2003, **42**, 3765–3771.
- 16 W. M. T. Gallerneault, F. Vnuk and R. W. Smith, *J. Appl. Phys.*, 1983, **54**, 4200–4201.
- 17 M. F. Fyhn, J. Chevallier, A. N. Larsen, R. Feidenhans and M. Seibt, *Phys. Rev. B: Condens. Matter Mater. Phys.*, 1999, **60**, 5770.
- 18 P. Kaghazchi, *J. Phys.: Condens. Matter*, 2013, **25**, 382204.
- 19 P. Kaghazchi, *J. Chem. Phys.*, 2013, **138**, 054706.
- 20 S. Sabet and P. Kaghazchi, *J. Chem. Phys.*, 2014, **140**, 191102.

